Dynamics of a Hysteretic Relay Oscillator with Periodic Forcing[*]

Tamás Kalmár-Nagy[†], Pankaj Wahi[‡], and Abhishek Halder[†]

Abstract. The dynamics of a hysteretic relay oscillator with simple harmonic forcing is studied in this paper. Even though there are no bounded solutions in the absence of forcing, periodic excitation gives rise to more complex responses including periodic, quasi-periodic, and chaotic behavior. A Poincaré map is introduced to facilitate mathematical analysis. Families of period-one solutions are determined as fixed points of the Poincaré map. These represent coexisting subharmonic responses. Conditions on the amplitude and frequency of the forcing for the existence of periodic solutions have been obtained. Linear stability analysis reveals that these solutions can be classified as centers or saddles. The presence of higher periodic or quasi-periodic motions together with homoclinic and heteroclinic tangles implies the existence of chaotic solutions.

Key words. hysteresis, relay oscillator, forced response, Poincaré map

AMS subject classifications. 34C25, 34C55, 70K40, 70K42, 70K43, 70K50

DOI. 10.1137/100784606

1. Introduction. Over the past decades, relay systems with hysteresis have attracted increasing attention. This class of nonlinear systems has found applications in a wide range of engineering problems including voltage regulators, DC motors, and servomechanisms [1, 2, 3, 4, 5, 6, 7]. Relays, in general, have two output branches, and the output of a relay jumps discontinuously whenever the input exceeds a certain critical value. For an ideal relay, there is a single critical value for which the output is discontinuous, while for a relay with hysteresis, there are two such critical input values, as shown in Figure 1(a).

Andronov and colleagues [2] and Åström [7] studied the existence and stability of period-one solutions (i.e., solutions having exactly two relay switchings per period). Gonçalves and coworkers [8, 9] presented a global analysis of relay systems using Lyapunov functions. Johansson, Rantzer, and Åström and di Bernardo and coworkers extensively studied different aspects of feedback systems with ideal relays (see [10, 11, 12] and references therein). Periodic solutions in a relay system with square-wave excitation was considered by Varigonda and Georgiou [3], while Fleishman [13] focused on periodic response under sinusoidal forcing. A related class of nonlinear systems involves relay operators with delays in the input. Barton, Krauskopf, and Wilson [14], Fridman, Fridman, and Shustin [15], and Norbury and Wilson [16] considered first order delayed relay systems while Bayer and Heiden [17], Sieber [18], Barton, Krauskopf, and Wilson [19], and Colombo et al. [20] studied second order systems. These

[†]Department of Aerospace Engineering, Texas A & M University, Ross Street, College Station, TX 77845 (kalmarnagy@aero.tamu.edu, a0h7710@aeromail.tamu.edu).

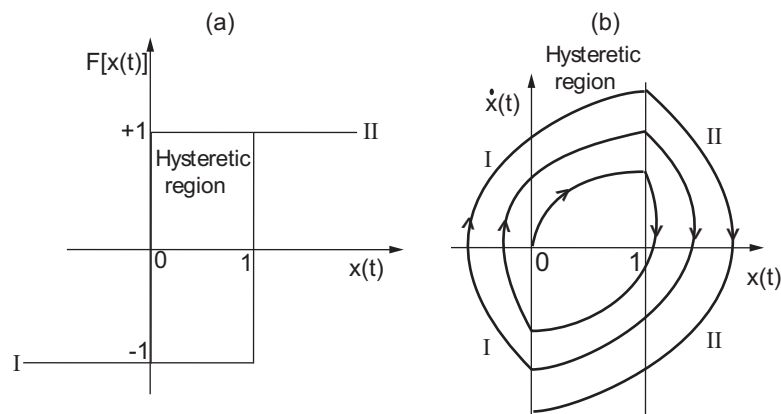[‡]Indian Institute of Technology Kanpur, Kanpur, India (wahi@iitk.ac.in).

Figure 1. (a) *The relay operator with hysteresis.* (b) *Phase portrait of* (1) *for* $A = 0$. *Initial conditions are* $x(0) = 0$ *and* $\dot{x}(0) = 0$. *See* (15)–(18).

studies include periodic solutions, their bifurcations, and chaotic solutions in these systems with or without forcing.

Hysteretic relay operators are also used in modeling complex hysteresis in materials where they are commonly known as the elementary Preisach operators [21, 22, 23, 24].

Relay systems belong to the general class of piecewise smooth dynamical systems. Other systems belonging to this class include systems with play or backlash [25], systems with friction [26, 27, 28, 29, 30], systems with impacts [26, 27, 28, 30, 31, 32, 33, 34, 35], and other hybrid systems [36, 37, 38, 39]. Leine and Nijmeijer [26] provide an overview and examples of bifurcation phenomena in such nonsmooth dynamical systems. In particular, the relay system considered in this study is a piecewise linear system which is similar to the much studied repeated impact of a ball with a sinusoidally vibrating table [31, 40, 41, 42, 43, 44, 45] and its Hamiltonian analogue studied in relevance to particle physics [46, 47, 48]. Further, the equation studied in this paper can also be taken as a simple model for automotive suspension with magneto-rheological (MR) damper under periodic forcing.

In this paper, we study the dynamics of a simple hysteretic relay operator under periodic excitation. The results reveal the unstable character of the negative hysteresis feedback. (Negative feedback is to be interpreted as negative energy dissipation due to the counterclockwise orientation of the relay diagram.) Each switching of the relay represents energy supply, which is responsible for a rich variety of dynamic responses ranging from periodic to chaotic solutions. We obtain conditions on the parameters, i.e., amplitude and frequency of the forcing for which bounded solutions can exist. To facilitate the analysis, we introduce a two-dimensional (2D) Poincaré map. Fixed points of the Poincaré map correspond to periodic solutions of the system. There are two families of period-one solutions corresponding to two families of fixed points of the Poincaré map. On the Poincaré plane, one family of fixed points corresponds to centers, while the other corresponds to saddles. There are invariant curves around the centers on the Poincaré plane which correspond to quasi-periodic solutions. The presence of homoclinic tangles has been shown numerically. This indicates the existence of chaotic solutions. As the parameters are varied, the centers and the saddles merge in a saddle-center bifurcation

[49, 50]. For these parameter values, there is a single family of nonhyperbolic fixed points corresponding to a single family of period-one solutions with no other bounded solutions.

2. Mathematical model of the relay oscillator. In this paper we study a simple model of a hysteretic relay oscillator. The "minimal" model (which would, for example, describe a bang-bang controlled mass under external forcing)

$$(1) \qquad \ddot{x}(t) + F[x(t)] = A\cos(\omega t + \phi), \qquad A \geq 0, \ \omega > 0, \ \phi \in (-\pi, \pi],$$

is expected to be useful for understanding more complicated systems with similar properties. Here A, ω, and ϕ are the amplitude, frequency, and phase of the forcing, respectively. The hysteretic relay operator $F[x(t)]$ (shown in Figure 1(a)) is defined as

$$(2) \qquad F[x(t)] = \begin{cases} -1, & x(t) \leq 0, \\ e, & 0 < x(t) < 1, \\ 1, & x(t) \geq 1. \end{cases}$$

This operator depends on the initial conditions and the time history of the solution $x(t)$; i.e., the discrete variable e is either -1 or 1, depending on whether the solution enters the hysteretic region $0 < x(t) < 1$ from the left or right. Without loss of generality, the initial conditions can be specified as

$$(3) \qquad x_I(0) = 0, \quad \dot{x}_I(0) = v_I, \quad e = -1.$$

When $F[x(t)] = \mp 1$, the evolution of the dynamical system is described by

$$(4) \qquad\qquad\qquad (I) \quad \ddot{x}_I(t) - 1 = A\cos(\omega t + \phi_I),$$

$$(5) \qquad\qquad\qquad (II) \quad \ddot{x}_{II}(t) + 1 = A\cos(\omega t + \phi_{II}),$$

where the subscripts are used to differentiate between the two subsystems. Figure 1(b) shows the phase portrait in $x(t)$ and $\dot{x}(t)$ for the free response of the system (i.e., $A = 0$; see section 4). The dynamics switches between the subsystems when the solution trajectories intersect $x_I(t) = 1$ from the left, i.e., $\dot{x}_I(t) \geq 0$, or $x_{II}(t) = 0$ from the right, i.e., $\dot{x}_{II}(t) \leq 0$.

To make the analysis simpler, time is reset when transition occurs between subsystems. To account for this artificial time-shift, the phase of the forcing is "updated" at the switchings. Therefore, the evolution of the dynamics is completely specified by

$$(6) \qquad \ddot{x}_I(t) - 1 = A\cos(\omega t + \phi_I), \qquad x_I(0) = 0, \ \dot{x}_I(0) = v_I, \ t \in [0, t_I],$$

$$(7) \qquad \ddot{x}_{II}(t) + 1 = A\cos(\omega t + \phi_{II}), \qquad x_{II}(0) = 1, \ \dot{x}_{II}(0) = v_{II}, \ t \in [0, t_{II}].$$

Here t_I and t_{II} are the switching times defined implicitly by $x_I(t_I) = 1$ and $x_{II}(t_{II}) = 0$, respectively.

3. The phase space and solutions. Figure 2(a) depicts the evolution of solution trajectories in $x(t)$, $\dot{x}(t)$, and $F[x(t)]$. Time t is introduced as another state variable resulting in an extended phase space [25, 31]. Clearly $x_I(t) \in X_I = (-\infty, 1]$ and $x_{II}(t) \in X_{II} = [0, \infty)$. Also, $\dot{x}_I(t), \dot{x}_{II}(t) \in \mathbb{R}$ and $t \in \mathbb{R}^+$. The extended phase space is therefore $X_I \times \mathbb{R} \times \mathbb{R}^+ \bigcup X_{II} \times \mathbb{R} \times \mathbb{R}^+$. This space is a proper subset of $\mathbb{R}^3 \times \{-1, 1\}$, where the discrete set $\{-1, 1\}$ is simply the range of $F[x(t)]$.

It is again emphasized in Figure 2 that the system consists of two distinct subsystems, viz. subsystem I and subsystem II. The dynamics of subsystem I switches to that of subsystem II
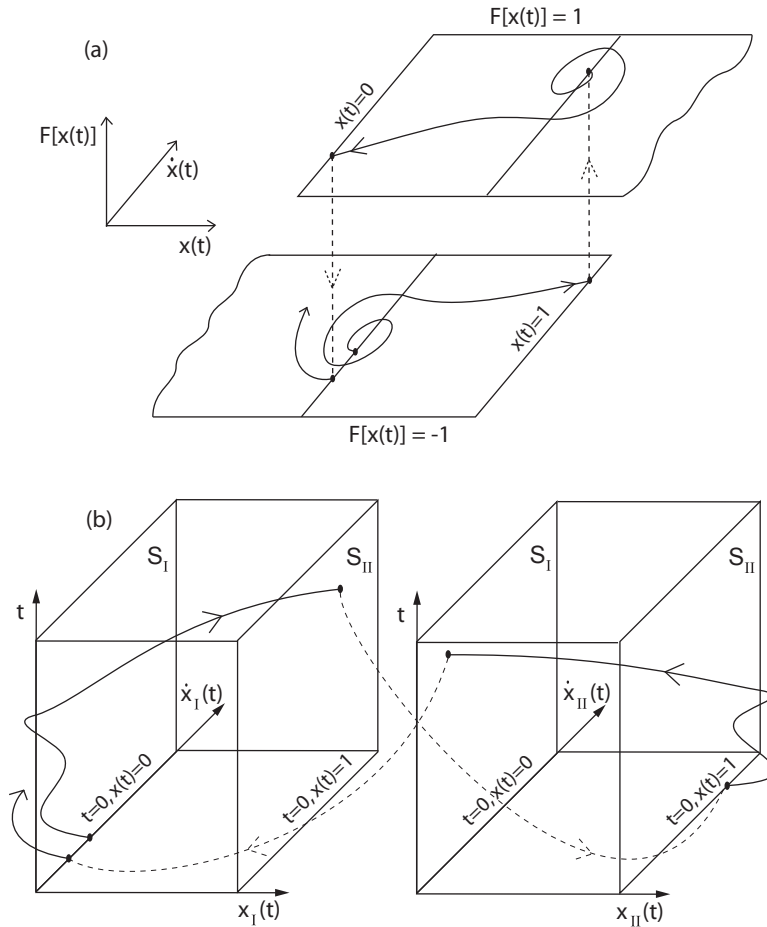
Figure 2. (a) *Phase space of* (1) *in* $x(t)$, $\dot{x}(t)$, *and* $F[x(t)]$. (b) *Extended phase space* $(x_I(t), \dot{x}_I(t), t) \bigcup$ $(x_{II}(t), \dot{x}_{II}(t), t)$.

when the solution trajectories intersect the surface $S_{II} = \{(\dot{x}(t), t) \mid x(t) = 1, \, \dot{x}(t) \geq 0\}$, and from subsystem II to subsystem I when they intersect the plane $S_I = \{(\dot{x}(t), t) \mid x(t) = 0,$ $\dot{x}(t) \leq 0\}$, as demonstrated in Figure 2(b).

Having described the structure of the phase space, we now turn our attention to the solutions. The solution of subsystem I can be written in closed form as

$$(8) \qquad x_I(t) = \frac{1}{2}t^2 + \left(v_I - \frac{A}{\omega}\sin(\phi_I)\right)t + \frac{A}{\omega^2}\cos(\phi_I) - \frac{A}{\omega^2}\cos(\omega t + \phi_I),$$

$$(9) \qquad \dot{x}_I(t) = t + v_I - \frac{A}{\omega}\sin(\phi_I) + \frac{A}{\omega}\sin(\omega t + \phi_I).$$

Similarly, the solution of subsystem II is

$$(10) \qquad x_{II}(t) = 1 - \frac{1}{2}t^2 + \left(v_{II} - \frac{A}{\omega}\sin(\phi_{II})\right)t + \frac{A}{\omega^2}\cos(\phi_{II}) - \frac{A}{\omega^2}\cos(\omega t + \phi_{II}),$$

$$(11) \qquad \dot{x}_{II}(t) = -t + v_{II} - \frac{A}{\omega}\sin(\phi_{II}) + \frac{A}{\omega}\sin(\omega t + \phi_{II}).$$

Note that the transformation $(v_I, \phi_I) \to (-v_{II}, \phi_{II} + \pi)$ in (8) and (9) is equivalent to

$$(12) \qquad (x_I(t), \dot{x}_I(t)) \to (1 - x_{II}(t), -\dot{x}_{II}(t)),$$

and the substitution $(v_{II}, \phi_{II}) \to (-v_I, \phi_I + \pi)$ in (10) and (11) leads to

$$(13) \qquad (x_{II}(t), \dot{x}_{II}(t)) \to (1 - x_I(t), -\dot{x}_I(t)).$$

Therefore a solution of one subsystem with an initial velocity v and initial phase of the forcing ϕ also represents solution trajectories of the other subsystem with the corresponding initial velocity $-v$ and initial phase $\phi + \pi$. As a consequence, solutions appear in pairs; i.e., if $(x(t), \dot{x}(t))$ is a solution of (1), then so is $(1 - x(t), -\dot{x}(t))$.

Having established some properties of the solutions, we proceed with our analysis of the model. First, the free response of the model is discussed.

4. Free response. In this section, we show that in the absence of forcing, i.e., $A = 0$, all solutions of the system are unbounded. This can be explained by noting that each switching of the relay corresponds to the injection of energy into the system.

The unforced system is given by

$$(14) \qquad \ddot{x}(t) + F[x(t)] = 0.$$

The solution of the subsystems I and II for this case becomes

$$(15) \qquad x_I(t) = \frac{1}{2} t^2 + v_I\, t,$$

$$(16) \qquad \dot{x}_I(t) = t + v_I$$

and

$$(17) \qquad x_{II}(t) = 1 - \frac{1}{2} t^2 + v_{II}\, t,$$

$$(18) \qquad \dot{x}_{II}(t) = -t + v_{II}.$$

When $x_I(t_I) = 1$, the system switches from subsystem I to subsystem II. The equation determining the switching time t_I is therefore

$$(19) \qquad \frac{1}{2} t_I^2 + v_I\, t_I - 1 = 0,$$

which can be solved in closed form to give (for $t_I > 0$)

$$(20) \qquad t_I = -v_I + \sqrt{v_I^2 + 2}\,.$$

Substituting t_I into (16), we get the velocity at the switching as

$$\dot{x}_I(t_I) = \sqrt{v_I^2 + 2}\,.$$

The initial velocity for the subsystem II is $\dot{x}_{II}(0) = v_{II} = \dot{x}_I(t_I)$. Substituting $v_{II} = \sqrt{v_I^2 + 2}$ into (17), the solution $x_{II}(t)$ is given by

$$(21) \qquad x_{II}(t) = 1 - \frac{1}{2}t^2 + \sqrt{v_I^2 + 2}\, t.$$

The switch from subsystem II to subsystem I occurs when $x_{II}(t_{II}) = 0$. This yields

$$(22) \qquad 1 - \frac{1}{2}t_{II}^2 + \sqrt{v_I^2 + 2}\, t_{II} = 0.$$

The above equation can again be solved in closed form (for $t_{II} > 0$) to give

$$(23) \qquad t_{II} = \sqrt{v_I^2 + 2} + \sqrt{v_I^2 + 4}\,.$$

Substituting t_{II} from (23) into (18), we get

$$(24) \qquad v_{II}(t_{II}) = -\sqrt{v_I^2 + 4}\,,$$

which is also the next initial velocity for subsystem I; i.e., $\dot{x}_I(0) = v_I = v_{II}(t_{II})$. From (24), we note that the absolute velocity of the system at switchings is monotonically increasing without bound. The phase portrait depicted in Figure 1(b) corresponds to the free response with $x(0) = 0$ and $\dot{x}(0) = v_I = 0$.

Next we consider the case $A > 0$. For a detailed analysis of the forced response, it is convenient to introduce a Poincaré map [25, 31] and study this discrete map instead of the continuous evolution of the system. In the next section, we compute the switching times that will be needed for obtaining the Poincaré map.

5. Switching times. In order to find the switching time t_I at which transition takes place between subsystems I and II, the switching criterion $x_I(t_I) = 1$ is substituted into (8), resulting in

$$(25) \qquad \frac{1}{2}t_I^2 + \left(v_I - \frac{A}{\omega}\sin(\phi_I)\right)t_I + \frac{A}{\omega^2}\cos(\phi_I) - \frac{A}{\omega^2}\cos(\omega t_I + \phi_I) - 1 = 0.$$

The switching time t_I is the first positive root of (25) and is a function of v_I and ϕ_I for fixed A and ω. Due to the transcendental nature of the equation, numerical solution is required. (Details of the numerical algorithm are provided in the appendix. It will be shown that when $A \leqslant 1$, the algorithm works irrespective of the value of ω.) The function $t_I(v_I, \phi_I)$ can have discontinuities corresponding to grazing bifurcations [51, 52] depending on the parameters A and ω. The velocity at the transition (from (9)) is

$$(26) \qquad \dot{x}_I(t_I) = t_I + v_I - \frac{A}{\omega}\sin(\phi_I) + \frac{A}{\omega}\sin(\omega t_I + \phi_I).$$

The phase of the forcing at the transition is simply

$$(27) \qquad \phi_I + \omega\, t_I \bmod 2\,\pi.$$

Similarly, to find the time t_{II} of the transition from subsystem II to subsystem I, the switching criterion $x_{II}(t_{II}) = 0$ is substituted into (10) to yield

$$(28) \qquad -\frac{1}{2}t_{II}^2 + \left(v_{II} - \frac{A}{\omega}\sin(\phi_{II})\right)t_{II} + \frac{A}{\omega^2}\cos(\phi_{II}) - \frac{A}{\omega^2}\cos(\omega t_{II} + \phi_{II}) + 1 = 0.$$

The switching time t_{II} is the smallest positive root of this equation. The velocity at the transition is (from (11))

$$(29) \qquad \dot{x}_{II}(t_{II}) = -t_{II} + v_{II} - \frac{A}{\omega}\sin(\phi_{II}) + \frac{A}{\omega}\sin(\omega t_{II} + \phi_{II}),$$

and the phase is $\phi_{II} + \omega\,t_{II} \bmod 2\,\pi$. From here on, the modulo 2π notation for the phase variable will not be explicitly written out.

Next, we outline the procedure for obtaining the discrete Poincaré map.

6. Poincaré map. With knowledge of the switching times, we are now in a position to construct a map to effectively study the behavior of solutions of (1). First, consider the mapping $(\dot{x}_I(0) = v_I, \phi_I) \to (\dot{x}_I(t_I), \phi_I + \omega\,t_I)$ of the initial velocity and phase to the velocity and phase at the time of the transition from subsystem I to subsystem II. Recall that the initial and final positions are uniquely specified by $x_I(0) = 0$ and $x_I(t_I) = 1$. As already mentioned in section 4, the final velocity and phase for the solution of subsystem I at the transition ((26) and (27)) will serve as initial velocity and phase for the solution of subsystem II, i.e.,

$$(30) \qquad v_{II} = \dot{x}_I(t_I) = t_I + v_I - \frac{A}{\omega}\sin(\phi_I) + \frac{A}{\omega}\sin(\phi_{II}),$$

$$(31) \qquad \phi_{II} = \phi_I + \omega\,t_I.$$

Similarly, the final values of the velocity and phase of the solution of subsystem II will provide the initial conditions for the solution of subsystem I as

$$(32) \qquad v_I = \dot{x}_{II}(t_{II}) = -t_{II} + v_{II} - \frac{A}{\omega}\sin(\phi_{II}) + \frac{A}{\omega}\sin(\phi_I),$$

$$(33) \qquad \phi_I = \phi_{II} + \omega\,t_{II}.$$

Rearranging (30) and (32) yields

$$(34) \qquad v_{II} - \frac{A}{\omega}\sin(\phi_{II}) = t_I + v_I - \frac{A}{\omega}\sin(\phi_I),$$

$$(35) \qquad v_I - \frac{A}{\omega}\sin(\phi_I) = -t_{II} + v_{II} - \frac{A}{\omega}\sin(\phi_{II}).$$

The form of these expressions motivates the introduction of a new variable, $z = v - \frac{A}{\omega}\sin(\phi)$.[1] Equations (34) and (35) can now be rewritten as

$$(36) \qquad z_{II} = t_I + z_I,$$

$$(37) \qquad z_I = -t_{II} + z_{II},$$

---

[1] z is the velocity component induced by the hysteretic force field $F[x(t)]$. It can also be viewed as the relative velocity between the solution trajectories of (1) with $F[x(t)]$ as defined in (2) with $F[x(t)] \equiv 0$.

where $z_I = v_I - \frac{A}{\omega}\sin(\phi_I)$ and $z_{II} = v_{II} - \frac{A}{\omega}\sin(\phi_{II})$. We can now relate initial values of the variables z, ϕ to their values at the switchings by the two maps Π_I, Π_{II} as

$$(38) \qquad \begin{pmatrix} z_{II} \\ \phi_{II} \end{pmatrix} = \Pi_I \begin{pmatrix} z_I \\ \phi_I \end{pmatrix} = \begin{pmatrix} z_I + t_I \\ \phi_I + \omega t_I \end{pmatrix},$$

$$(39) \qquad \begin{pmatrix} z_I \\ \phi_I \end{pmatrix} = \Pi_{II} \begin{pmatrix} z_{II} \\ \phi_{II} \end{pmatrix} = \begin{pmatrix} z_{II} - t_{II} \\ \phi_{II} + \omega t_{II} \end{pmatrix}.$$

To specify the range and domain of these maps, we introduce the Poincaré surfaces $\Sigma_I = \{(z_I, \phi_I) \mid x(t) = 0\}$ and $\Sigma_{II} = \{(z_{II}, \phi_{II}) \mid x(t) = 1\}$. Clearly, Π_I and Π_{II} are maps from Σ_I onto Σ_{II} and from Σ_{II} onto Σ_I, respectively. The Poincaré map (or return map) Π is now defined as the map of the plane Σ_I onto itself after a pair of switchings. The map Π is therefore obtained by composing the two maps Π_{II} and Π_I as

$$(40) \qquad \Pi \begin{pmatrix} z_I \\ \phi_I \end{pmatrix} = \Pi_{II} \circ \Pi_I \begin{pmatrix} z_I \\ \phi_I \end{pmatrix}.$$

Substituting (38) and (39) for Π_I and Π_{II} in (40) results in

$$(41) \qquad \Pi \begin{pmatrix} z_I \\ \phi_I \end{pmatrix} = \begin{pmatrix} z_I + t_I(z_I, \phi_I) - t_{II}(z_I, \phi_I) \\ \phi_I + \omega t_I(z_I, \phi_I) + \omega t_{II}(z_I, \phi_I) \end{pmatrix}.$$

Equation (41) defines the Poincaré map Π to be used in the subsequent analysis. The implicit dependence of the switching times t_I and t_{II} on (z_I, ϕ_I) is also emphasized. With the new variables z_I and z_{II} introduced in (25) and (28), the switching times t_I and t_{II} are determined as the first positive roots of

$$(42) \qquad \frac{1}{2}t_I^2 + z_I t_I + \frac{A}{\omega^2}\cos(\phi_I) - \frac{A}{\omega^2}\cos(\omega t_I + \phi_I) - 1 = 0,$$

$$(43) \qquad -\frac{1}{2}t_{II}^2 + z_{II} t_{II} + \frac{A}{\omega^2}\cos(\phi_{II}) - \frac{A}{\omega^2}\cos(\omega t_{II} + \phi_{II}) + 1 = 0,$$

respectively. Substituting z_{II} and ϕ_{II} from (36) and (31) into (43) results in

$$(44) \qquad -\frac{1}{2}t_{II}^2 + (z_I + t_I)t_{II} + \frac{A}{\omega^2}\cos(\phi_I + \omega t_I) - \frac{A}{\omega^2}\cos(\phi_I + \omega t_I + \omega t_{II}) + 1 = 0.$$

Equations (42) and (44) now define the implicit dependence of t_I and t_{II} on (z_I, ϕ_I). As mentioned previously, the switching times are not necessarily continuous functions of the parameters, and depending on the parameters A and ω, the switching times t_I and t_{II} can in general have discontinuities corresponding to grazing bifurcations [51, 52] as z_I and ϕ_I are varied. This will result in a discontinuous Poincaré map, leading to further complexity of the system. However, in this work, we consider only parameter values A and ω for which the switching times and consequently the Poincaré map are continuous.

    With the introduction of the Poincaré map we have reduced the study of the original hybrid system (1) to that of the discrete map $\Pi : \Sigma_I \to \Sigma_I$. The inverse of the Poincaré

map (which is used in section 8 to compute backward iterations) can be simply obtained by reversing time and appropriately changing initial conditions. This yields

$$(45) \qquad \Pi^{-1}\begin{pmatrix} z_I \\ \phi_I \end{pmatrix} = \Pi_I^{-1} \circ \Pi_{II}^{-1}\begin{pmatrix} z_I \\ \phi_I \end{pmatrix} = \begin{pmatrix} z_I - t_I + t_{II} \\ \phi_I - \omega\, t_I - \omega\, t_{II} \end{pmatrix},$$

where the switching times are now defined by the equations

$$(46) \qquad \begin{aligned} 1 + \frac{1}{2}\, t_I^2 - z_{II}\, t_I + \frac{A}{\omega^2}\cos(-\phi_{II}) - \frac{A}{\omega^2}\cos(\omega\, t_I - \phi_{II}) &= 0, \\ \frac{1}{2}\, t_{II}^2 + z_I\, t_{II} - \frac{A}{\omega^2}\cos(-\phi_I) + \frac{A}{\omega^2}\cos(\omega\, t_{II} - \phi_I) + 1 &= 0. \end{aligned}$$

In the following section, we proceed to study the periodic solutions of the system.

7. Periodic solutions. We first locate period-one solutions of (1), i.e., solutions which involve a single pair of switchings between Σ_I and Σ_{II}. Equivalently, we are looking for the fixed points of the Poincaré map Π.

7.1. Period-one solutions. Fixed points of the Poincaré map are given by

$$\begin{pmatrix} z_I^* \\ \phi_I^* \end{pmatrix} = \Pi\begin{pmatrix} z_I^* \\ \phi_I^* \end{pmatrix} = \begin{pmatrix} z_I^* + t_I - t_{II} \\ \phi_I^* + \omega\, t_I + \omega\, t_{II} \end{pmatrix}.$$

These equations result in

$$(47) \qquad t_I = t_{II} = \frac{n\,\pi}{\omega}, \qquad n \in \mathbb{Z}^+.$$

Having obtained the switching times t_I and t_{II} for a fixed point of the Poincaré map, the values of z_I^* and ϕ_I^* can be easily determined to yield two families of fixed points of the Poincaré map for a given set of parameters A and ω ($\omega^2 \le 2A$) as

$$(48) \qquad (z_I^*, \phi_I^*)_{1,2} = \left(-\frac{n\,\pi}{2\,\omega}, \pm\arccos\left(\frac{\omega^2}{2A}\right) \right), \qquad n = 1, 3, 5, \ldots.$$

Each of these fixed points corresponds to a period-one solution of (1). The $x(t)$-$\dot{x}(t)$ portraits of the system corresponding to $n = 1$, 3, 5, and 7 are shown in Figure 3. These different period-one motions represent $1 : n$ subharmonic resonances of the system, and they coexist for a given set of parameter values. The period-one solutions shown in Figure 3 corresponding to $(-\pi/2, \pi/3)$, $(-\pi/2, -\pi/3)$, $(-3\pi/2, \pi/3)$, and $(-3\pi/2, -\pi/3)$ are plotted together in Figure 4 to emphasize their coexistence. The initial conditions for each $x(t)$-$\dot{x}(t)$ portrait have been chosen to be consistent with the fixed points given in (48); i.e., for $A = 1$, $\omega = 1$, and $n = 1$, the initial conditions corresponding to $z_I = -\pi/2$ and $\phi_I = -\pi/3$ are $x(0) = 0$ and $\dot{x}(0) = -\pi/2 - \sqrt{3}/2$.

Having obtained the conditions for the existence of period-one solutions of the system governed by (1), or equivalently the fixed points of the Poincaré map (41), we perform stability analysis of these fixed points in the next section.
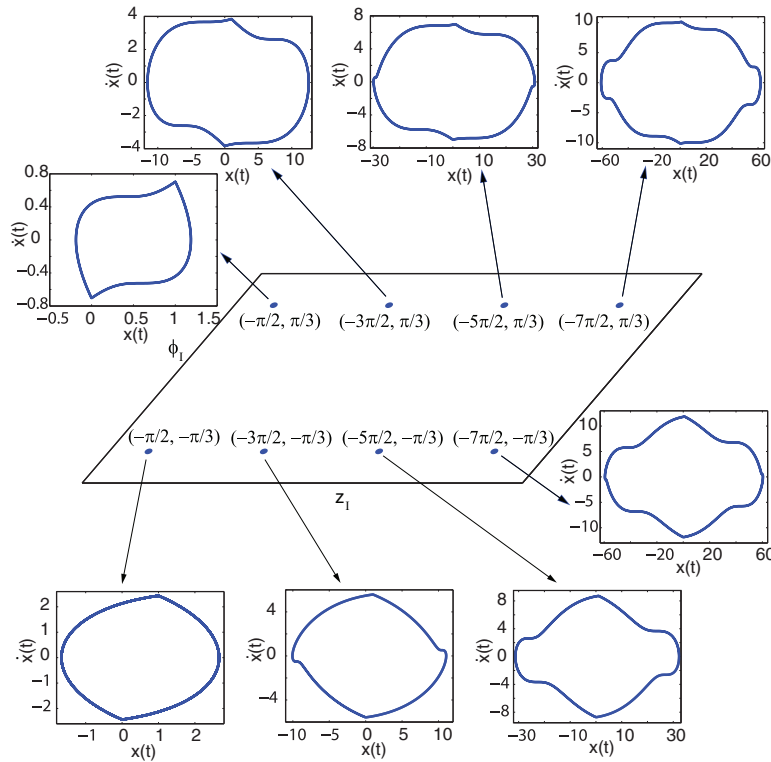
Figure 3. $x(t)$-$\dot{x}(t)$ portraits for $A = 1$ and $\omega = 1$ corresponding to the fixed points of the Poincaré map for $n = 1$, 3, 5, and 7.

7.2. Stability analysis of period-one solutions. For the purpose of stability analysis of the fixed points of the Poincaré map (41), we calculate the linearized Poincaré map about the fixed points (z_I^*, ϕ_I^*) using a perturbation expansion. The linearized Poincaré map $D\Pi$ of map (41) can be written as

$$(49) \qquad D\Pi = \left. \begin{pmatrix} 1 + \frac{\partial t_I}{\partial z_I} - \frac{\partial t_{II}}{\partial z_I} & \frac{\partial t_I}{\partial \phi_I} - \frac{\partial t_{II}}{\partial \phi_I} \\ \omega \left(\frac{\partial t_I}{\partial z_I} + \frac{\partial t_{II}}{\partial z_I} \right) & 1 + \omega \left(\frac{\partial t_I}{\partial \phi_I} + \frac{\partial t_{II}}{\partial \phi_I} \right) \end{pmatrix} \right|_{(z_I^*, \phi_I^*)}.$$

The derivatives are obtained by differentiating (42) and (44). The eigenvalues of the matrix $D\Pi$ determine the stability of the fixed points of the Poincaré map (41) or equivalently the period-one solutions of the system (1). The eigenvalues of $D\Pi$ are given by

$$(50) \qquad \lambda_{1,2} = \frac{\operatorname{Tr} D\Pi}{2} \pm \frac{\sqrt{(\operatorname{Tr} D\Pi)^2 - 4 \det(D\Pi)}}{2}.$$

Simple calculations yield

$$(51) \qquad \operatorname{Tr} D\Pi = 2 + \frac{32 A n \pi \sin \phi}{(n\pi - 2A \sin \phi)^2},$$
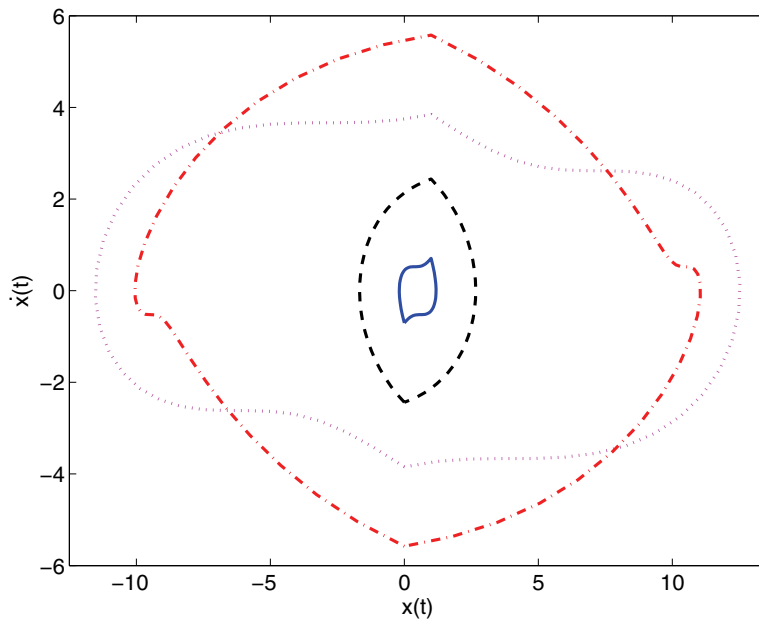
$$(52) \qquad \det(D\Pi) = 1.$$

Figure 4. $x(t)$-$\dot{x}(t)$ portraits for $A = 1$ and $\omega = 1$ corresponding to the fixed points $(-\pi/2, \pi/3)$ (solid line), $(-\pi/2, -\pi/3)$ (dashed line), $(-3\pi/2, \pi/3)$ (dotted line), and $(-3\pi/2, -\pi/3)$ (dash-dotted line).

Since $\lambda_1 \lambda_2 = \det(D\Pi) = 1$, there are three possibilities for the eigenvalues:

1. Both λ_1 and λ_2 are real and distinct. In this case, one has a modulus greater than one (eigenvalue outside the unit circle) and the other smaller than one (eigenvalue inside the unit circle). This fixed point is a saddle.
2. λ_1 and λ_2 are complex conjugate with $|\lambda_1| = |\lambda_2| = 1$ (eigenvalues on the unit circle). The fixed point is a center.
3. Either $\lambda_1 = \lambda_2 = 1$ or $\lambda_1 = \lambda_2 = -1$. The fixed point is a nonhyperbolic fixed point, and nonlinear analysis is required to determine the behavior of the fixed point.

From (50), we note that the eigenvalues $\lambda_{1,2}$ are real and distinct if $|\operatorname{Tr} D\Pi| > 2$, and they are complex conjugate if $|\operatorname{Tr} D\Pi| < 2$. Equation (51) then implies that the family of fixed points corresponding to $\phi_I^* = \arccos\left(\frac{\omega^2}{2A}\right)$ and $\phi_I^* = -\arccos\left(\frac{\omega^2}{2A}\right)$ are saddles and centers, respectively. These two branches of period-one solutions are shown in Figure 5. In the limiting case of $\omega^2 = 2A$, the two branches merge in a saddle-center bifurcation [49, 50], leaving a single family of fixed points

$$(z_I^*, \phi_I^*) = \left(\frac{-n\pi}{2\sqrt{2A}}, 0\right), \qquad n = 1, 3, 5, \ldots.$$

At these points both the eigenvalues are equal to 1.

7.3. Higher-period and quasi-periodic solutions. In this section, we illustrate the procedure for a period-two solution only. The procedure for higher periodic solutions is similar. A period-two solution of (1) is a fixed point of the map Π^2. The sequence of switching times for (1) is denoted as $t_I, t_{II}, t_{III}, t_{IV}, \ldots$. Denoting the fixed point of the map Π^2 as (z_I^{**}, ϕ_I^{**}),
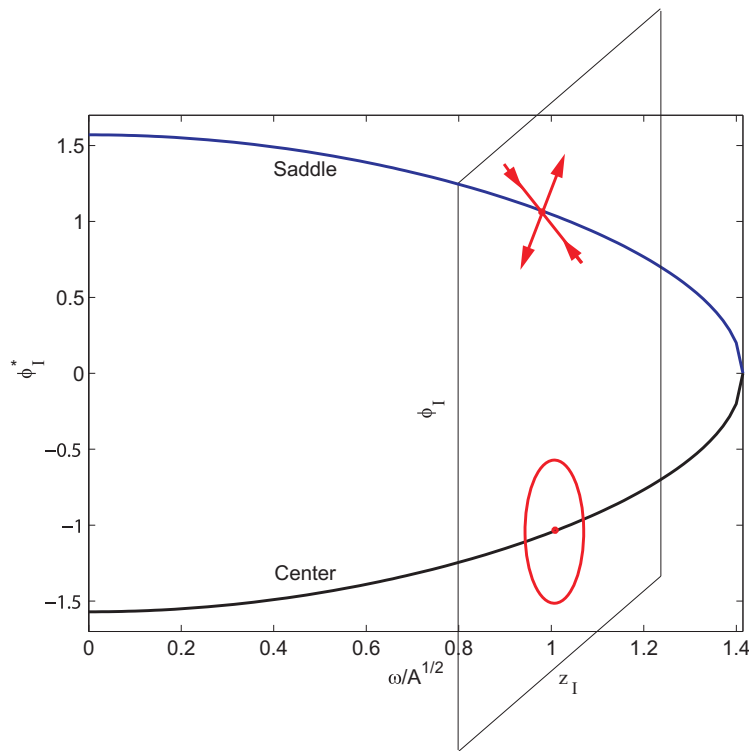
Figure 5. *The two branches of fixed points of the Poincaré map* (41).

from (41) we have

$$\begin{pmatrix} z_I^{**} \\ \phi_I^{**} \end{pmatrix} = \Pi \circ \Pi \begin{pmatrix} z_I^{**} \\ \phi_I^{**} \end{pmatrix} = \begin{pmatrix} z_I^{**} + t_I - t_{II} + t_{III} - t_{IV} \\ \phi_I^{**} + \omega \left(t_I + t_{II} + t_{III} + t_{IV} \right) \end{pmatrix}.$$

From the above, we get two equations,

$$t_I - t_{II} + t_{III} - t_{IV} = 0 \tag{53}$$

and

$$\omega \left(t_I + t_{II} + t_{III} + t_{IV} \right) = 2 \, n \, \pi \tag{54}$$

for some integer n. We require four more equations in order to be able to solve for the six unknowns z_I^{**}, ϕ_I^{**}, t_I, t_{II}, t_{III}, and t_{IV}. These equations come from the four switching criteria, $x_I(t_I) = 1$, $x_{II}(t_{II}) = 0$, $x_I(t_{III}) = 1$, and $x_{II}(t_{IV}) = 0$. Substituting for the appropriate initial conditions in each case, the latter equations are given by

$$(55) \qquad \frac{1}{2}t_I^2 + z_I^{**}t_I + \frac{A}{\omega^2}\cos(\phi_I^{**}) - \frac{A}{\omega^2}\cos(\phi_I^{**} + \omega t_I) - 1 = 0,$$

$$(56) \qquad -\frac{1}{2}t_{II}^2 + (z_I^{**} + t_I)\,t_{II} + \frac{A}{\omega^2}\cos(\phi_I^{**} + \omega t_I) - \frac{A}{\omega^2}\cos(\phi_I^{**} + \omega t_I + \omega t_{II}) + 1 = 0,$$

(57)
$$\frac{1}{2}t_{III}^2 + (z_I^{**} + t_I - t_{II})\,t_{III} + \frac{A}{\omega^2}\cos(\phi_I^{**} + \omega t_I + \omega t_{II}) - \frac{A}{\omega^2}\cos(\phi_I^{**} + \omega t_I + \omega t_{II} + \omega t_{III}) - 1 = 0,$$

$$-\frac{1}{2}t_{IV}^2 + (z_I^{**} + t_I - t_{II} + t_{III})\,t_{IV} + \frac{A}{\omega^2}\cos(\phi_I^{**} + \omega t_I + \omega t_{II} + \omega t_{III})$$
$$(58) \qquad \qquad - \frac{A}{\omega^2}\cos(\phi_I^{**} + \omega t_I + \omega t_{II} + \omega t_{III} + \omega t_{IV}) + 1 = 0.$$

Equations (53)–(58) need to be solved for the six unknowns z_I^{**}, ϕ_I^{**}, t_I, t_{II}, t_{III}, and t_{IV} numerically. In our simulations, we found no period-two solutions. However, we found four period-three solutions, which are shown in Figure 6. These period-three solutions appear in pairs, as noted previously. Solutions a and b form a center-type pair, while solutions c and d form a saddle-type pair. This is concluded from the numerical evaluation of the eigenvalues of the linearized Poincaré map, i.e., the Floquet multipliers associated with the numerically obtained period-three solution pair. These solution pairs have the symmetry defined by (12) and (13) as $(x_b(t), \dot{x}_b(t)) = (1 - x_a(t), \dot{x}_a(t))$ and $(x_a(t), \dot{x}_a(t)) = (1 - x_b(t), \dot{x}_b(t))$, where the subscripts a and b are used to refer to the solutions a and b in Figure 6. We also found other higher odd period solution pairs and some even period solution pairs. The phase portrait corresponding to the period-eight solution obtained for $A = 1$ and $\omega = 1/2$ is shown in Figure 7(a). It has been observed numerically that there are invariant curves surrounding the center (as depicted in Figure 5). These curves correspond to quasi-periodic solutions of (1). The trajectory of (1) in the $x(t)$-$\dot{x}(t)$ plane corresponding to a quasi-periodic trajectory for the first few cycles is shown in Figure 7(b).

8. Global dynamics. The presence of centers and saddles on the Poincaré plane hints towards possible homoclinic and heteroclinic orbits or tangles. The dynamics of the system in the z-ϕ variables on the Poincaré plane for $A = 1$ and $\omega = 1$ is shown in Figure 8. Here we have shown the dynamics around the first three centers and saddles. The eigenvector for the first saddle is also plotted in the figure and matches well with the numerically observed directions of the stable and unstable manifolds of the saddle. While it seems that there is a homoclinic orbit around the center, the unstable and the stable manifolds of the saddles intersect transversally, giving rise to chaotic tangles. A zoomed view of the boxed portion of Figure 8(bottom) is shown in Figure 8(top). Also shown are the approximate heteroclinic connections between the saddle-type period-three solution pair. The presence of several higher-period solution pairs hints towards the existence of a Smale horseshoe [31, 53] related to the transverse intersection of the stable and unstable manifolds of the saddle. In Figure 9, we have plotted the result of forward and backward iterations of 250×250 points in a small neighborhood of the saddle. To compute the backward iterations, the inverse Poincaré map presented in section 7 is used. The transverse intersection of the stable and the unstable manifolds of the saddle is clearly
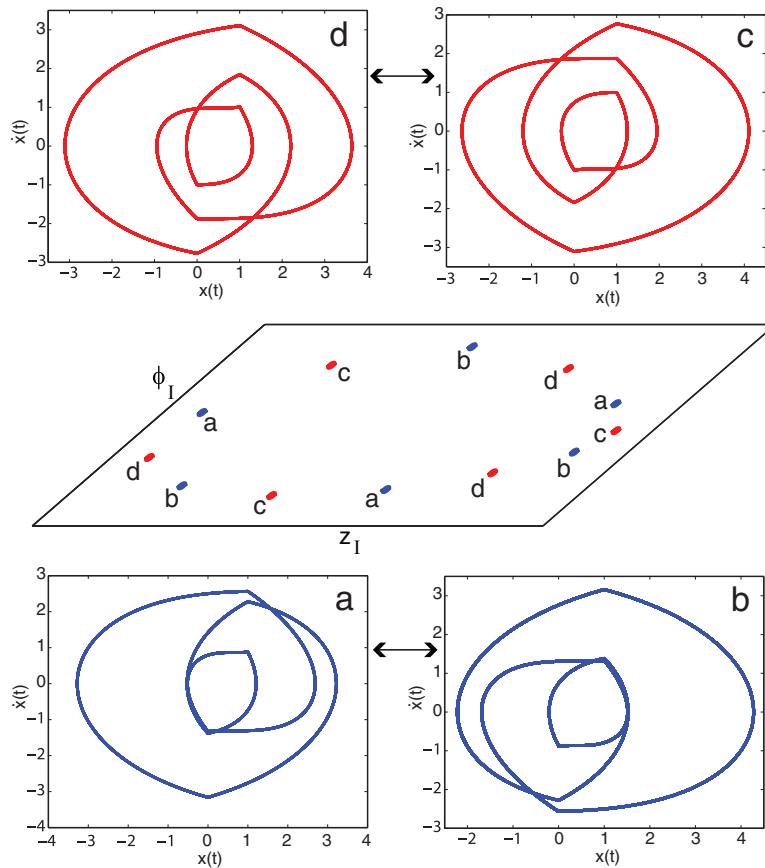
Figure 6. $x(t)$-$\dot{x}(t)$ *portraits of the period-three solutions of* (1) *for* $A = 1$ *and* $\omega = 1$.
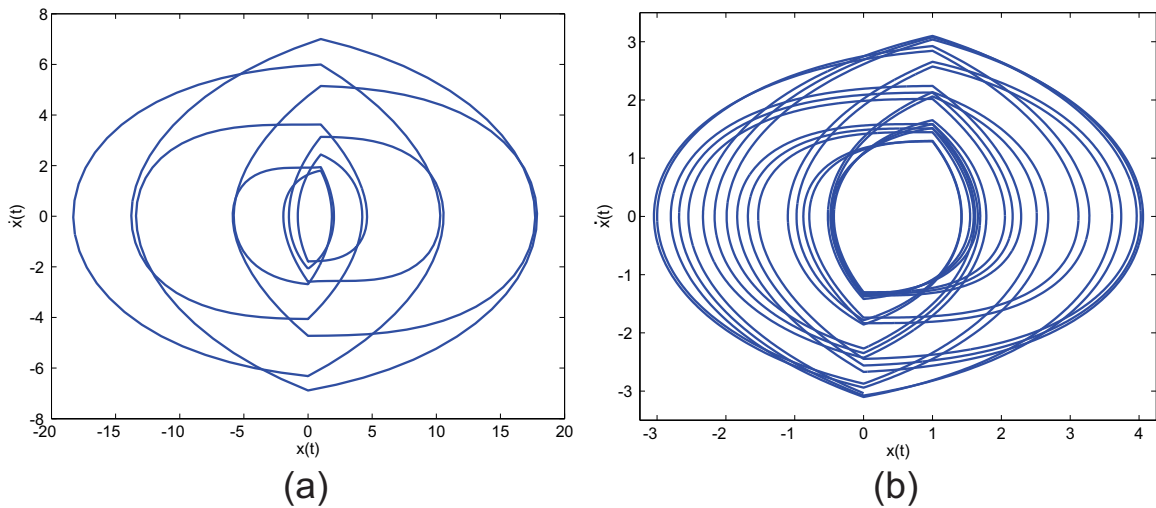

Figure 7. (a) $x(t)$-$\dot{x}(t)$ *portrait of the period-eight solution of* (1) *for* $A = 1$ *and* $\omega = 1/2$. *Initial conditions:* $z_I = -0.1328$ *and* $\phi_I = -1.3325$. (b) $x(t)$-$\dot{x}(t)$ *portrait corresponding to a quasi-periodic solution of* (1) *for* $A = 1$ *and* $\omega = 1$. *Initial conditions correspond to* $z_I = -0.97$ *and* $\phi_I = -\pi/3$, *i.e.,* $x(0) = 0$ *and* $\dot{x}(0) = -1.83$.
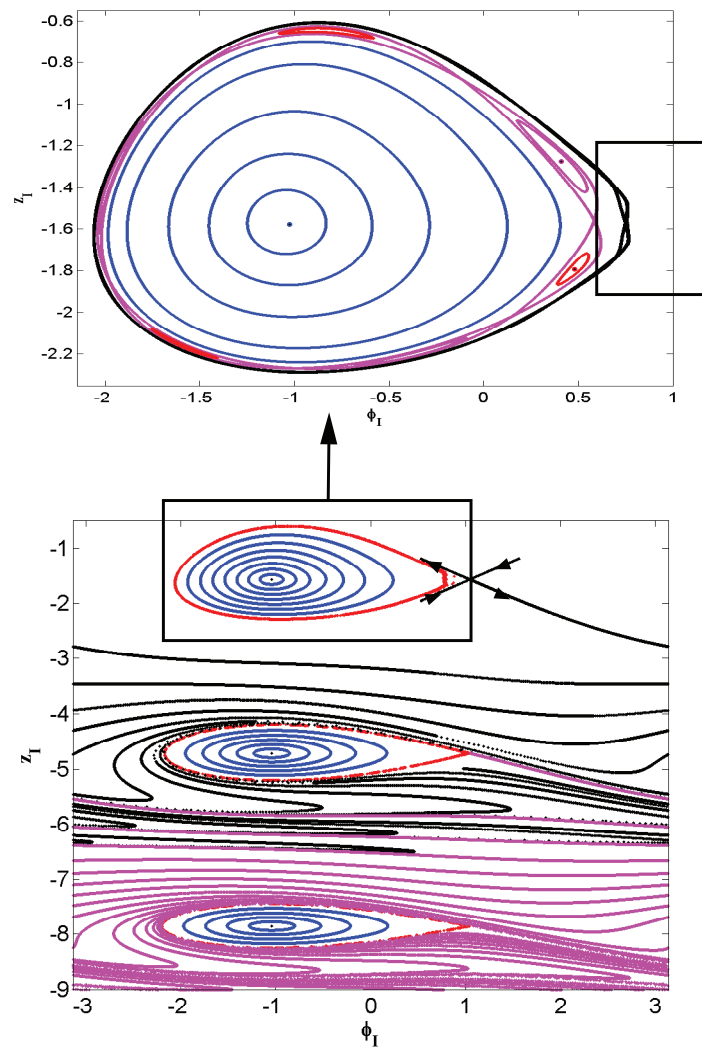
Figure 8. *Dynamics around the first three centers and saddles in the ϕ_I-z_I plane for $A = 1$ and $\omega = 1$. Boxed region in the top panel is expanded in Figure* 9.

visible in Figure 9. This numerical evidence shows the existence of a Smale horseshoe, which implies the existence of an infinite number of higher periodic and bounded aperiodic solutions.

At the saddle-center bifurcation point, we have a single family of nonhyperbolic fixed points on the Poincaré plane.

9. Conclusions. Dynamics of a system with a hysteretic relay operator with simple harmonic forcing was studied in this paper. A Poincaré map was introduced to facilitate the analysis. Conditions on the amplitude and frequency of the forcing for the existence of periodic solutions were obtained. There are two families of period-one solutions determined as the fixed points of the Poincaré map. On the Poincaré plane, one family of the fixed points is a center and the other one is a saddle. Higher-period solutions were obtained numerically.
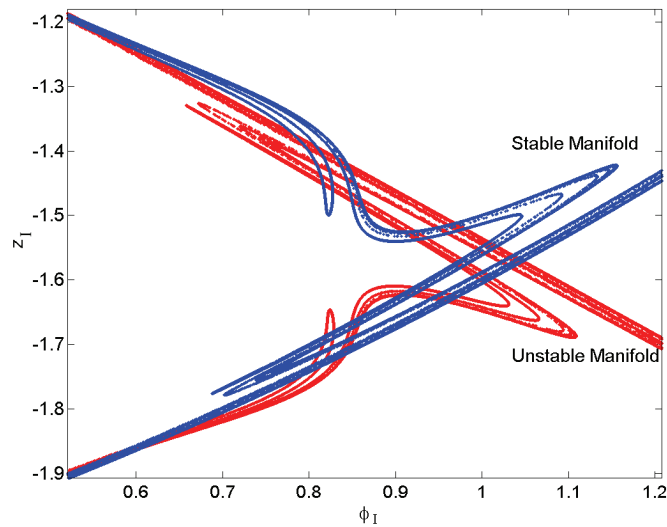
Figure 9. *Dynamics in the ϕ_I-z_I plane for $A = 1$ and $\omega = 1$ showing transverse intersection of the stable and unstable manifolds of the saddle. The region corresponds to the boxed region in Figure 8(top).*

Invariant curves surrounding the center on the Poincaré plane were obtained which correspond to quasi-periodic solutions. Homoclinic and heteroclinic tangles were observed numerically, implying the presence of chaotic solutions.

Appendix. Algorithm to obtain the first positive root of a second order polynomial containing a cosine term. The first positive root of (25) and (28) can be obtained by forward marching in time with a suitably chosen time step, as in [45]. To obtain the first root with sufficient numerical accuracy, the time step required might be very small when there are two roots close to each other, which renders the time-marching algorithm inefficient. This motivates the development of an algorithm wherein we identify disjoint intervals which can contain only a single root and use standard numerical root-finding algorithms like the bisection method in these intervals to locate the roots therein.

The switching conditions, (25) and (28), can be written in a general form as

$$(59) \qquad a\,t^2 + b\,t + c - d\cos(\omega\,t + \phi) \;=\; 0.$$

First we reduce the number of free parameters in (59) by dividing throughout by d and scaling time as $\tau = \omega\,t$. This reduces (59) to

$$(60) \qquad a_1\,\tau^2 + b_1\,\tau + c_1 - \cos(\tau + \phi) \;=\; 0,$$

where $a_1 = \frac{a}{d\,\omega^2}$, $b_1 = \frac{b}{d\,\omega}$, and $c_1 = \frac{c}{d}$. The first root t of (59) is related to the first root τ of (60) as $t = \frac{\tau}{\omega}$. The algorithm for reliably obtaining the first root of (60) can be summarized as follows:

1. The first step involves identifying the intervals in which the roots of (60) can possibly exist. To determine these intervals, (60) is rewritten as $f(\tau) - g(\tau) = 0$, where $f(\tau) = a_1\,\tau^2 + b_1\,\tau + c_1$ and $g(\tau) = \cos(\tau + \phi)$. Since $|g(\tau)| \leq 1$, feasible intervals for the roots

of $f(\tau) - g(\tau) = 0$ are determined by the roots of $f(\tau) \pm 1 = 0$. We define the set of real positive roots of $f(\tau) \pm 1 = 0$ as $R = \{r_i \in \mathbb{R}^+ \mid f(r_i) \pm 1 = 0\}$. The feasible intervals are now determined by the cardinality of the set R (denoted by $n(R)$) along with the members of R as follows. For $n(R) = 0$, there are no real positive roots of $f(\tau) - g(\tau) = 0$. For $n(R) > 0$, the feasible intervals for the roots are given by $[0, r_1]$ for $n(R) = 1$, $[r_1, r_2]$ for $n(R) = 2$, $[0, r_1] \bigcup [r_2, r_3]$ for $n(R) = 3$, and $[r_1, r_2] \bigcup [r_3, r_4]$ for $n = 4$, where $0 < r_1 < r_2 < r_3 < r_4$.

2. Each of the feasible intervals for the roots of $f(\tau) - g(\tau) = 0$ determined in the previous step can have multiple roots. The next step in the algorithm, therefore, involves partitioning the above intervals into subintervals (not necessarily of equal length) such that each subinterval can have exactly one root. But this can happen only if the function is monotonic in that subinterval. To ensure this, we use the fact that a function is monotonic in the interval in which its derivative has the same sign and, hence, can have only one root in that interval. This requirement can be met if somehow we can guarantee that our "target subinterval" (which we seek to obtain in such a way that it contains either zero or exactly one root) contains exactly one inflexion point of the slopes.

   Thus, we simply need to compute the zeros of the second derivative of the function and then construct the subintervals such that each subinterval contains exactly one zero of the second derivative; hence exactly one inflexion point of the first derivative, and hence the monotonicity of the function itself, is guaranteed. As a result, now the bisection algorithm can be applied, as we already know that the subinterval on which we are applying the bisection contains at most one root. To perform the above partition, we proceed as follows:

   (a) Since $f''(\tau) = 2\,a_1$ and $g''(\tau) = -\cos(\tau + \phi)$, the roots of $f''(\tau) - g''(\tau) = 0$ can be obtained in closed form (for $|a_1| \leq \frac{1}{2}$) as

   $$\tau_{dd} = 2\,m\,\pi \pm (\arccos(-2\,a_1) - \phi), \quad m = 0, 1, 2, \ldots.$$

   For $|a_1| > \frac{1}{2}$, $f''(\tau) - g''(\tau) = 0$ has no real roots. The roots τ_{dd} along with the endpoints of the feasible intervals provide a partition of the feasible intervals into feasible subintervals such that $f'(\tau) - g'(\tau) = 0$ can have only one root in each subinterval. It can be noted that all numerical simulations given in this paper accord with the condition $|a_1| \leq \frac{1}{2}$; namely, the forcing amplitude is chosen in a way such that it does not exceed unity.

   (b) The existence of roots of $f'(\tau) - g'(\tau) = 0$ in the subintervals determined in the previous step is ascertained by evaluating $f'(\tau) - g'(\tau)$ at the endpoints of the subinterval. If the value is zero at either of the endpoints, that endpoint is the root τ_d of $f'(\tau) - g'(\tau) = 0$. If the function $f'(\tau) - g'(\tau)$ changes sign at the endpoints, there is a root τ_d in the subinterval which can be obtained using the bisection method; otherwise there is no root in that subinterval. The roots τ_d of $f'(\tau) - g'(\tau) = 0$ in each of the subintervals along with the endpoints of the feasible intervals form a partition of the feasible intervals into subintervals such that $f(\tau) - g(\tau) = 0$ can have only one root in each subinterval.

3. Having obtained subintervals of the semireal axis $\mathbb{R}^+$ such that there can be exactly one root of the function $f(\tau) - g(\tau) = 0$ in each subinterval, each subinterval is checked for the roots analogous to the procedure described for the roots of $f'(\tau) - g'(\tau)$ in the previous step. The procedure starts with the first subinterval and is terminated if either a root is obtained or all the subintervals are exhausted, in which case there are no real positive roots of (60).

Acknowledgment. We would like to thank the reviewers for their valuable comments and suggestions for improving the paper.

REFERENCES

[1] YA. Z. TSYPKIN, *Relay Control Systems*, Cambridge University Press, Cambridge, UK, 1984.

[2] A. A. ANDRONOV, A. A. VITT, AND S. E. KHAIKIN, *Theory of Oscillators*, Dover Publications, New York, 1966.

[3] S. VARIGONDA AND T. T. GEORGIOU, *Dynamics of relay relaxation oscillators*, IEEE Trans. Automat. Control, 46 (2001), pp. 65–77.

[4] ZH. T. ZHUSUBALIEV AND V. S. TITOV, *Chaotic oscillations in the relay system with hysteresis*, Autom. Remote Control, 62 (2001), pp. 55–66.

[5] N. S. POSTNIKOV, *Dynamic chaos in relay systems with hysteresis*, Comput. Math. Model., 8 (1997), pp. 62–72.

[6] ZH. T. ZHUSUBALIEV AND E. A. SOUKHOTERIN, *Oscillations in a relay control system with hysteresis and time dead zone*, Math. Comput. Simulation, 58 (2002), pp. 329–350.

[7] K. J. ÅSTRÖM, *Oscillations in systems with relay feedback*, in Adaptive Control, Filtering, and Signal Processing, K. J. Åström, G. C. Goodwin, and P. R. Kumar, eds., Springer-Verlag, New York, 1995, pp. 1–25.

[8] J. M. GONÇALVES, A. MEGRETSKI, AND M. A. DAHLEH, *Global stability of relay feedback system*, IEEE Trans. Automat. Control, 46 (2001), pp. 550–562.

[9] J. M. GONÇALVES, A. MEGRETSKI, AND M. A. DAHLEH, *Global analysis of piecewise linear systems using impact maps and surface Lyapunov functions*, IEEE Trans. Automat. Control, 48 (2003), pp. 2089–2106.

[10] K. H. JOHANSSON, A. RANTZER, AND K. J. ÅSTRÖM, *Fast switches in relay feedback systems*, Automatica, 35 (1999), pp. 539–552.

[11] M. DI BERNARDO, K. H. JOHANSSON, AND F. VASCA, *Self-oscillations and sliding in relay feedback systems: Symmetry and bifurcations*, Internat. J. Bifur. Chaos Appl. Sci. Engrg., 11 (2001), pp. 1121–1140.

[12] M. DI BERNARDO, K. H. JOHANSSON, U. JÖNSSON, AND V. FRANCESCO, *On the robustness of periodic solutions in relay feedback systems*, in Proceedings of the Fifteenth IFAC Triennial World Congress, Barcelona, Spain, 2002, Elsevier Science, Oxford, UK, 2003.

[13] B. A. FLEISHMAN, *Forced oscillations and convex superposition in piecewise-linear systems*, SIAM Rev., 7 (1965), pp. 205–222.

[14] D. A. W. BARTON, B. KRAUSKOPF, AND R. E. WILSON, *Explicit periodic solutions in a model of a relay controller with delay and forcing*, Nonlinearity, 18 (2005), pp. 2637–2656.

[15] E. FRIDMAN, L. FRIDMAN, AND E. SHUSTIN, *Steady modes in relay control systems with time delay and periodic disturbances*, ASME J. Dyn. Syst. Meas. Control, 122 (2000), pp. 732–737.

[16] J. NORBURY AND R. E. WILSON, *Dynamics of constrained differential delay equations*, J. Comput. Appl. Math., 125 (2000), pp. 201–215.

[17] W. BAYER AND U. HEIDEN, *Oscillation types and bifurcations of a nonlinear second-order differential-difference equation*, J. Dynam. Differential Equations, 10 (1998), pp. 303–326.

[18] J. SIEBER, *Dynamics of delayed relay systems*, Nonlinearity, 19 (2006), pp. 2489–2527.

[19] D. A. W. BARTON, B. KRAUSKOPF, AND R. E. WILSON, *Periodic solutions and their bifurcations in a non-smooth second-order delay differential equation*, Dynam. Systems, 21 (2006), pp. 289–311.

[20] A. Colombo, M. di Bernardo, S. J. Hogan, and P. Kowalczyk, *Complex dynamics in a hysteretic relay feedback system with delay*, J. Nonlinear Sci., 17 (2007), pp. 85–108.

[21] I. D. Mayergoyz, *Mathematical Models of Hysteresis and Their Applications*, Elsevier, New York, 2003.

[22] M. A. Krasonoselśkii and A. V. Pokrovskii, *Systems with Hysteresis*, Springer-Verlag, Berlin, 1983.

[23] P. D. Spanos, A. Kontsos, and P. Cacciola, *Steady-state dynamic response of Preisach hysteretic systems*, ASME J. Vibration Acoustics, 128 (2006), pp. 244–250.

[24] P. Krejči, *Forced oscillations in Preisach systems*, Phys. B, 275 (2000), pp. 81–86.

[25] M. Kleczka, E. Kreuzer, and W. Schiehlen, *Local and global stability of a piecewise linear oscillator*, Philos. Trans. Roy. Soc. London Ser. A, 338 (1992), pp. 533–546.

[26] R. I. Leine and H. Nijmeijer, *Dynamics and Bifurcations of Non-Smooth Mechanical Systems*, Springer, New York, 2004.

[27] M. Kunze, *Non-Smooth Dynamical Systems*, Springer, New York, 2000.

[28] B. Brogliato, *Nonsmooth Mechanics: Models, Dynamics and Control*, Springer, New York, 1999.

[29] M. Oestreich, N. Hinrichs, and K. Popp, *Bifurcation and stability analysis for a non-smooth friction oscillator*, Arch. Appl. Mech., 66 (1996), pp. 301–314.

[30] N. Hinrichs, M. Oestreich, and K. Popp, *Dynamics of oscillators with impact and friction*, Chaos Solitons Fractals, 8 (1997), pp. 535–558.

[31] J. Guckenheimer and P. Holmes, *Nonlinear Oscillations, Dynamical Systems, and Bifurcations of Vector Fields*, Springer-Verlag, New York, 2002.

[32] E. E. Pavlovskaia and M. Wiercigroch, *Two dimensional map for impact oscillator with drift*, in Proceedings of the IUTAM Symposium on Chaotic Dynamics and Control of Systems and Processes in Mechanics, Springer, Norwell, MA, 2005, pp. 305–312.

[33] J. Ing, E. E. Pavlovskaia, and M. Wiercigroch, *Dynamics of a nearly symmetrical piecewise linear oscillator close to grazing incidence: Modelling and experimental verification*, Nonlinear Dynam., 46 (2006), pp. 225–238.

[34] W. Chin, E. Ott, H. E. Nusse, and C. Grebogi, *Grazing bifurcations in impact oscillators*, Phys. Rev. E, 50 (1994), pp. 4427–4444.

[35] S. W. Shaw and P. J. Holmes, *A periodically forced piecewise linear oscillator*, J. Sound Vibration, 90 (1983), pp. 129–155.

[36] J. Lygeros, K. H. Johansson, S. N. Simic, J. Zhang, and S. Sastry, *Dynamical properties of hybrid automata*, IEEE Trans. Automat. Control, 48 (2003), pp. 2–17.

[37] M. K. Oishi, I. M. Mitchell, A. M. Bayen, and C. J. Tomlin, *Hybrid system verification: Application to user-interface design*, IEEE Trans. Control Systems Tech., 16 (2008), pp. 229–244.

[38] R. G. Sanfelice, R. Goebel, and A. R. Teel, *A feedback control motivation for generalized solutions to hybrid systems*, in Hybrid Systems: Computation and Control, Lecture Notes in Comput. Sci. 3927, Springer, New York, 2006, pp. 522–536.

[39] R. Alur, T. A. Henzinger, and E. D. Sontag, *Hybrid Systems* III. *Verification and Control*, Springer-Verlag, Berlin, 1996.

[40] P. J. Holmes, *The dynamics of repeated impacts with a sinusoidally vibrating table*, J. Sound Vibration, 84 (1982), pp. 173–189.

[41] L. D. Pustylinikov, *Stable and oscillating motions in nonautonomous dynamical systems*, Trans. Moscow Math. Soc., 34 (1977), pp. 1–101.

[42] L. A. Wood and K. P. Byrne, *Experimental investigation of a random repeated impact process*, J. Sound Vibration, 85 (1982), pp. 53–69.

[43] A. C. J. Luo and R. P. S. Han, *The dynamics of a bouncing ball with a sinusoidally vibrating table revisited*, Nonlinear Dynam., 10 (1996), pp. 1–18.

[44] C. N. Bapat and S. Sankar, *Repeated impacts on a sinusoidally vibrating table reappraised*, J. Sound Vibration, 108 (1986), pp. 99–115.

[45] N. B. Tufillaro, T. Abbott, and J. P. Reilly, *An Experimental Approach to Nonlinear Dynamics and Chaos*, Addison–Wesley, New York, 1992.

[46] B. V. Chirikov, *A universal instability of many dimensional oscillator systems*, Phys. Rep., 52 (1979), pp. 263–379.

[47] J. M. Greene, *A method for determining a stochastic transition*, J. Math. Phys., 20 (1980), pp. 1183–1201.

[48] A. J. Lichtenberg and M. A. Lieberman, *Regular and Chaotic Dynamics*, Springer-Verlag, New York, 1992.

[49] V. G. Gelfreich, *Splitting of a small separatrix loop near the saddle-center bifurcation in area-preserving maps*, Phys. D, 136 (2000), pp. 266–279.

[50] D. C. Diminnie and R. Haberman, *Slow passage through homoclinic orbits for the unfolding of a saddle-center bifurcation and the change in the adiabatic invariant*, Phys. D, 162 (2002), pp. 34–52.

[51] H. Dankowicz and X. Zhao, *Local analysis of co-dimension-one and co-dimension-two grazing bifurcations in impact microactuators*, Phys. D, 202 (2005), pp. 238–257.

[52] P. Kowalczyk, M. di Bernardo, A. R. Champneys, S. J. Hogan, P. T. Piiroinen, Yu. A. Kuznetsov, and A. Nordmark, *Two-parameter discontinuity-induced bifurcations of limit cycles: Classification and open problems*, Internat. J. Bifur. Chaos Appl. Sci. Engrg., 16 (2006), pp. 601–629.

[53] S. Smale, *Differentiable dynamical systems*, Bull. Amer. Math. Soc., 73 (1967), pp. 747–817.